AIAA JOURNAL
Vol. 37, No. 9, September 1999

Algorithm to Integrate the Ffowcs Williams–Hawkings Equation on Supersonic Rotating Domain

Sandro Ianniello*
Centro Italiano Ricerche Aerospaziali, 81043 Capua, Italy

The numerical solution of the Ffowcs Williams–Hawkings equation (Ffowcs Williams, J. E., and Hawkings, D. L., "Sound Generation by Turbulence and Surfaces in Arbitrary Motion," *Philosophical Transactions of the Royal Society*, Vol. A264, No. 1151, 1969, pp. 321–342) on a rotating supersonic domain is discussed. Based on the emission-surface algorithm, the adopted solver performs the integration on the so-called acoustic domain to avoid the Doppler singularity in the integral kernels. The presence of multiple emission times for the supersonic source points and the particular time evolution of the integration domain force the use of a particular data-fitting procedure on both the geometrical and integral quantities. The algorithm may be used in the numerical prediction of the quadrupole source term for helicopter rotors operating at a high transonic regime and in the aeroacoustic analysis of the modern propeller blades, rotating at supersonic tip speed.

Introduction

SINCE the end of the 1970s, when the importance of nonlinear terms was highlighted in the numerical estimation of noise from a high tip speed rotating blade, a change in the development and the application of theoretical and computational methodologies for the aeroacoustic analysis of helicopter rotors has occurred. Because of the requirement for a three-dimensional integration and the presence of the Doppler singularity in the integral kernels, the adoption of the Ffowcs Williams–Hawkings (FW–H)[1] equation for the numerical prediction of the high-speed impulsive (HSI) noise has always been considered difficult and computationally expensive. Over the past 15 years, interest of the aeroacoustic community has progressively moved toward alternative solution forms, such as the Kirchhoff approach[2] and the computational aeroacoustics methods,[3] relegating the acoustic analogy approach to the role of a linear problem solver. Actually, the computation of the nonlinear terms is a very difficult task. The delocalization of the shock waves off the blade tip arising at $M_{\text{tip}} \geq 0.88$ forces the extention of the computing domain beyond the sonic cylinder, where the Doppler factor prevents the usual FW–H solvers from achieving a reliable prediction of noise. From a theoretical point of view, the problem may be simply bypassed through the use of the emission-surface algorithms, where the integrals are determined on the blade retarded configuration, and the Doppler singularity does not appear in the integral kernels. Recently, a new method has been proposed and successfully implemented,[4] where the calculations proceed forward with respect to time, thus avoiding the solution of the retarded-time equation and the effects of the Doppler singularity. The emission-surface approach rarely has been used: The occurrence of multiple emission times in the supersonic region causes unconnected patches to appear, which temporarily link together into a single domain, following a time evolution, which is very difficult to numerically model.

Very interesting results concerning the integration on the acoustic surface have been published by Wells[5,6] and Wells and Han.[7] In these papers the need for determining, at each time step, a new computational grid with a clustering of the integration points along some particular critical radii was recognized, and very smooth signatures were obtained in the determination of the FW–H linear terms from a rectangular rotor blade and a propfan-type blade rotating at supersonic tip speed. Wells provides a detailed discussion of the mathematical aspects of the problem and points out the important differences in the computation of the acoustic planform for a rectangular and a swept blade. Neverthless, it is not clear how the numerical procedure accounts for the presence of unconnected regions; besides, to the author's knowledge, the method has never been applied to evaluate the quadrupole source term for helicopter rotors at delocalized conditions.

Both the retarded-time[8] and the emission-surface[9] algorithms have been recently used in the computation of the HSI noise from a hovering rotor. In particular, Farassat and Brentner[9] have developed a new integral formulation for the supersonic quadrupole source term, which has been successfully implemented in the code WOPWOP2+. Based on the far-field approximation and the use of a marching-cubes algorithm, these recent computations show how the noise contribution arising from the supersonic region affects the resulting noise waveform, increasing the width of the signature and its own asymmetrical shape. Nevertheless, especially for the most critical condition ($M_{\text{tip}} = 0.925/0.95$), the numerical predictions are affected by large fluctuations, which increase with the spanwise extension of the computing grid.

A new algorithm is presented to integrate the FW–H equation outside the sonic cylinder. Through a prescribed classification of the grid stations along span and a suitable data-fitting procedure, the new computational tool is able to provide an accurate reconstruction of the retarded domain in the presence of the multiple emission times. The integration is performed by a subdivision of the supersonic grid into different patches, whose exact identification allows the treatment of the particular time steps when the acoustic domain is constituted by unconnected regions. The code KURGAN has been successfully tested in the determination of the thickness noise from a supersonic tip speed blade and the HSI noise prediction from a hovering rotor.

Mathematical Aspects

Most numerical codes devoted to the aeroacoustic analysis of rotating blades are based on the well-known FW–H equation

$$c_0^2 \Box^2 \tilde{\rho} = \Box^2 p' = \frac{\bar{\partial}}{\partial t}[\rho_0 v_n \delta(f)] - \frac{\bar{\partial}}{\partial x_i}[\tilde{p}\hat{n}_i \delta(f)] + \frac{\bar{\partial}^2}{\partial x_i \partial x_j}\{T_{ij} H(f)\} \tag{1}$$

where p' is the acoustic pressure disturbance, $T_{ij} = \rho u_i u_j + (\tilde{p} - c_0^2 \tilde{\rho})$ is the Lighthill stress tensor, and the Heaviside function in the third term on the right-hand side points out that this source term vanishes inside the body (characterized by the equation $f = 0$). Through the use of the Green function technique, Eq. (1) is

Received 1 April 1998; presented as Paper 98-2378 at the AIAA/CEAS 4th Aeroacoustics Conference, Toulouse, France, 2–4 June 1998; revision received 10 December 1998; accepted for publication 31 January 1999.

*Research Engineer, Aeroacoutics Branch.

usually changed into an integral one, suitable for numerical implementation; nevertheless, depending on the adopted variable transformation, the integral resolution forms exhibit very different and interesting features. Brentner[10] has provided an exhaustive description of the possible forms of the acoustic integrals, suggesting classifying the corresponding numerical algorithms into retarded-time, collapsing-sphere, and emission-surface algorithms. In the following, we will limit our attention to the emission-surface algorithms, where the integration is performed on the time-dependent domain traced by all of the source points at their retarded positions. Furthermore, the analysis will be focused on the particular resolution forms implemented in the code, as regards the monopole and the quadrupole source terms.

The evaluation of the linear terms of Eq. (1) is usually achieved through the well-known Farassat formulation 1A (Ref. 11); nevertheless, the monopole term may be also computed through the following equation:

$$4\pi p'_T(\boldsymbol{x}, t) = \frac{\partial}{\partial t} \iint_{\Sigma} \left[\frac{\rho_0 v_n}{r\Lambda} \right]_{\tau^*} \mathrm{d}\Sigma \tag{2}$$

where $\Lambda = (1 + M_n^2 - 2M_n \cos\theta)^{1/2}$ and M_n is the projection of the Mach number along a direction normal to the blade surface. The only singularity $\Lambda = 0$ occurs when $M_n = 1$ and $\cos\theta = 0$ simultaneously and has been proved to be integrable by Farassat.[12] The $\Lambda = 0$ singularity represents a much less restrictive condition than the Doppler singularity affecting the retarded-time algorithms as formulation 1A.

Originally proposed by Yu et al.,[13] the far-field approximation allows the determination of the nonlinear term of the FW–H equation by a preliminary integration of the Lighthill stress tensor along the direction normal to the rotor plane. By the assumption that (observer time and location fixed) all of the source points placed along this direction have the same emission times, the quadrupole volume integrals may be reduced to some surface integrals, where the third space variable collapses into the term

$$Q_{ij} = \int_n T_{ij}\, \mathrm{d}n \tag{3}$$

This approximation is rigorously valid for in-plane and far-field observer locations and has been implemented in the following form[14]:

$$4\pi p'_Q(\boldsymbol{x}, t) = \frac{1}{c_0^2} \frac{\partial^2}{\partial t^2} \iint_{\Sigma} \left[\frac{Q_{rr}}{r} \right]_{\tau^*} \mathrm{d}\Sigma + \frac{1}{c_0} \frac{\partial}{\partial t} \iint_{\Sigma} \left[\frac{3Q_{rr} - Q_{ii}}{r^2} \right]_{\tau^*} \mathrm{d}\Sigma + \iint_{\Sigma} \left[\frac{3Q_{rr} - Q_{ii}}{r^3} \right]_{\tau^*} \mathrm{d}\Sigma \tag{4}$$

Recently, Farassat and Brentner[9] have developed a new integral formulation for the supersonic quadrupole sources (formulation Q2, Ref. 9), where the time derivatives appearing in Eq. (4) have been moved inside the integral sign. This manipulation could be very useful. The resulting noise waveforms computed through the emission-surface algorithms are often affected by a lot of pronounced oscillations. As argued by Wells,[7] this behavior does not arise because the time derivatives of Eq. (4) are taken outside instead of inside the integrals: It essentially depends on the integration itself and the difficulties in modeling the Σ surface. Nevertheless, any small fluctuation affecting the computed integrals is dramatically amplified by the subsequent time derivatives, so that the direct use of Eq. (4) may be considered a kind of reliability test for the algorithm devoted to the calculation of the retarded domain.

With observer time t and location $\boldsymbol{x}(t)$ fixed, the emission time τ^* represents the instant when the contribution of the source point [located at $\boldsymbol{y}(\tau^*)$] starts to reach the observer. The calculation of the emission time is performed through an iterative procedure, solving the equation

$$\tau = t - \frac{r}{c_0} = t - \frac{|\boldsymbol{x} - \boldsymbol{y}(\boldsymbol{\eta}, \tau)|}{c_0} = \Phi(\tau) \tag{5}$$

where $\boldsymbol{\eta}$ is the coordinate vector of source point in the body frame of reference. By the starting from the initial time $\tau = t$ and the corresponding positive value $f(\tau) = r/c_0$, the research for the root of the function $f(\tau) = [\tau - \Phi(\tau)]$ proceeds iteratively. When solved for a subsonic source point, Eq. (5) always exhibits a single root, whose determination may be considered a rather simple task. However, the calculation for supersonic sources is more difficult because a single observer time may correspond to three different emission times. The phenomenon is related to the finite value of the sound speed: whereas the contribution starting at τ_1^* runs toward the observer, the supersonically moving source point emits again and, depending on the observer–source relative position, three different signatures may reach the $\boldsymbol{x}$ observer location simultaneously. Figure 1 shows two typical $f(\tau)$ curves for a supersonic source with multiple emission times at two subsequent observer times ($t_2 > t_1$). Note that the midroots τ_2 are the only ones corresponding to a negative value of the first τ derivative f_τ, whereas the other two roots correspond to a positive value of f_τ and are characterized by a different sign of the second τ derivative $f_{\tau\tau}$ [related to the $f(\tau)$ curvature in the root point]. These differences are very important for the numerical procedure because they allow the recognition of some separate and well-defined regions of the retarded domain. The sign of the second τ-derivative

$$f_{\tau\tau} = \frac{\partial^2 f}{\partial \tau^2} = \dot{M}_i \hat{r}_i + \frac{c_0}{r}\left(M_r^2 - M^2\right)$$

is related to the curvature of the retarded domain. Figure 2 shows the subsonic region of the acoustic surface as computed for the untwisted, $\frac{1}{7}$th scaled UH-1H blade, rotating counterclockwise at $M_{\mathrm{tip}} = 1.5$ and an observer placed in the rotor plane (at 10 diameters from the rotor hub). The notable broadening is due to the different curvatures of the leading and trailing edges at the retarded configuration and occurs at their own crossing through the separation line $f_{\tau\tau} = 0$. The observer times corresponding to this wide retarded domain are characterized by the highest noise emission in the far field.

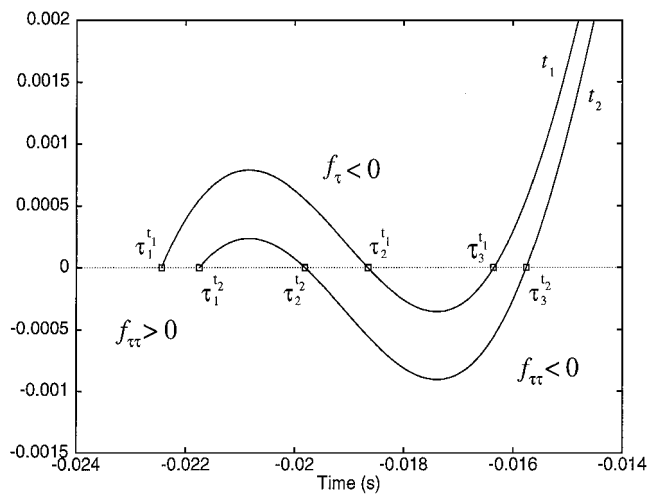

Fig. 1 Two subsequent ($t_2 > t_1$) $f(\tau)$ curves for a supersonic source point with three different emission times.

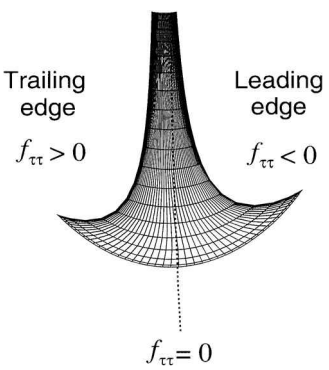

Fig. 2 Subsonic patch of the acoustic surface (UH-1H hovering blade at $M_{\mathrm{tip}} = 1.5$); broadening due to the different sign of $f_{\tau\tau}$ at the blade leading and trailing edges.

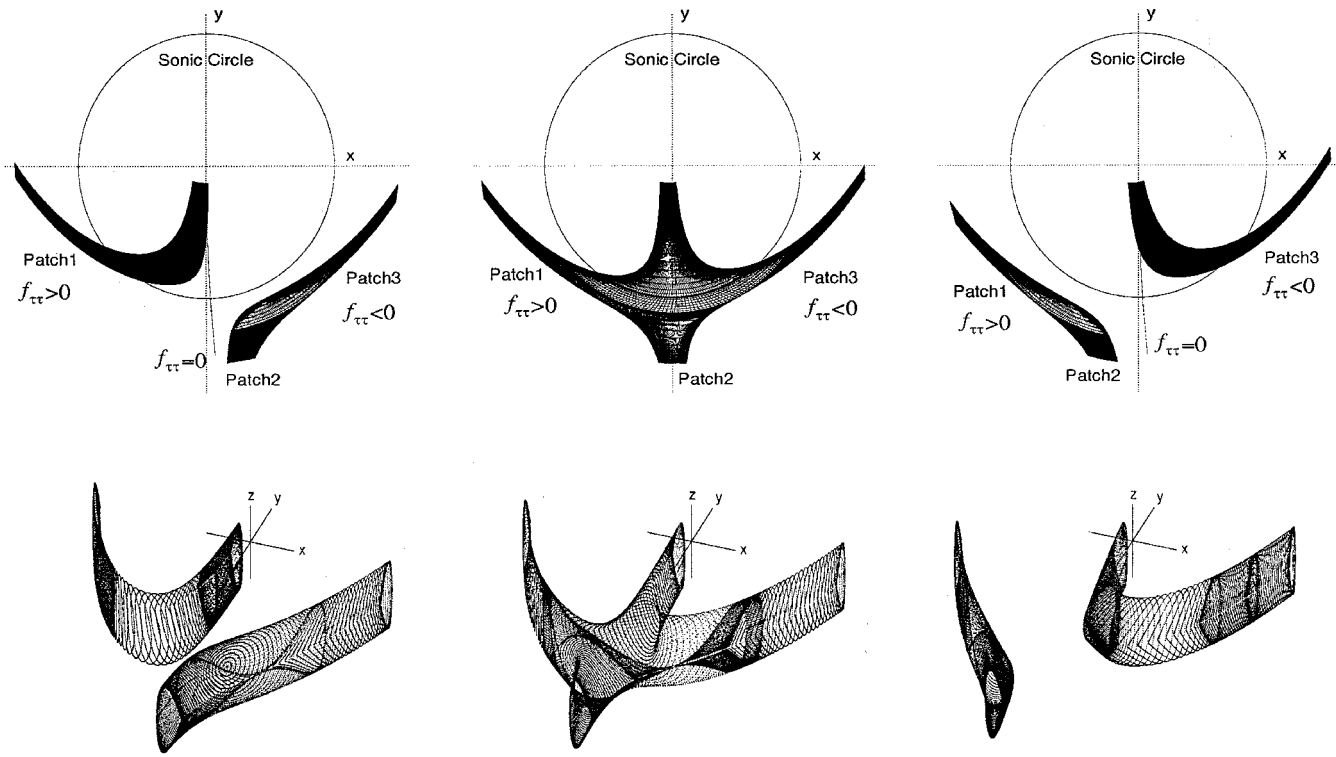

Fig. 3 Top and three-dimensional views of the acoustic surface for the hovering UH-1H blade at $M_{tip} = 1.5$, at three subsequent observer times; observer is placed in the rotor plane, at a distance of 10 diameters from the rotor hub ($x_{obs} = 20.9$, $Y_{obs} = Z_{obs} = 0$).

By the extending of the computations outside the sonic circle, the $f_{\tau\tau}$ plays a fundamental role because by means of its sign the code may identify the different supersonic patches. Figure 3 shows the acoustic surface at three subsequent observer times: Supersonic patches 1 and 3 are characterized by all source points with $f_{\tau\tau} > 0$ and $f_{\tau\tau} < 0$, respectively. In Fig. 3, the condition $f_\tau = 1 - M_r < 0$ is verified by all of the source points constituting patch 2, which exhibits some very interesting features. Unlike the supersonic regions 1 and 3, which at subsequent time steps rotate counterclockwise (as the blade), patch 2 seems to move in the opposite direction; this behavior also appears in Fig. 1, where the τ_2^{t1} root runs toward the subsequent τ_2^{t2} value moving oppositely with respect to the time axis. Furthermore, the source points of patch 2 undergo a topological inversion, as clearly shown in the three-dimensional views of the retarded domain (Fig. 3).

Supersonic Acoustic Surface

Starting from the original grid and determining all of the possible multiple emission times for the supersonic region, the retarded domain may appear as a sort of random distribution of points, whose location depends on both the computing grid and the kinematic conditions. The fundamental task of the numerical procedure is to order this distribution in such a manner as to have a regular grid to perform the integration.

The presence of three emission times should suggest the existence of three different supersonic patches; as a matter of fact, the acoustic domain usually appears as a single or a double region, at most constituted by two unconnected patches. On the other hand, the geometry of the retarded domain strongly depends on the geometry of the present grid; for example, it will be shown later how, starting from a swept planform, the acoustic surface may exhibit a kind of progressively broadening hole, which makes the integration domain very challenging to model. An accurate building of the acoustic surface requires a data-fitting procedure. The interpolation must be performed for two main reasons. The first is that the different spanwise stations of the computational grid may exhibit (at each observer time) a different number of multiple emission times; then, the interpolation allows the number of source points to be fixed on all of the stations to achieve a regular panelization of the acoustic domain. The second is a more physical reason: the fitting of data allows the linkage of the unconnected supersonic patches into the actual retarded configuration, thus providing for the discrete representation of a continuous line (the station) with a finite number of nodes. Unfortunately, the interpolation cannot be performed on the original grid. In fact, because of the notable widening of the retarded domain occurring outside the blade tip and a kind of flight of the source points from the Doppler line, the data-fitting procedure must suitably modify the computing grid at each time step. Ultimately, a self-adaptive scheme is required to build the integration domain.

Supersonic Patches

The capability to model some unconnected patches of the integration domain and to account for their temporary reconnection into a complex geometry is the fundamental feature of the numerical tool. This task is achieved through a suitable classification of the grid stations along span at their own retarded position. Note that the term station should rigorously refer to all of the source points of the numerical domain at the same kinematic conditions (in particular, for the hovering blade, at the same rotational velocity: $\boldsymbol{V} = \Omega \times \boldsymbol{r}$); nevertheless, in the evaluation of the supersonic thickness noise we will refer to the blade station as a particular NACA 0012 airfoil along the span. With the observer time and location fixed, each supersonic station may experience four different retarded conditions (depending on the kinematic conditions).

1) At the "supersonic" condition, all of the source points on the station exhibit three emission times.

2) A multiple region exists at the "mixed" condition, including the airfoil leading or trailing edge.

3) A multiple region exists at the "partial" condition, but it does not include either the leading or trailing edge.

4) At the "single" condition, the station has no source points with multiple emission times.

By assembling the similar stations into separate patches, the code is able to identify and split the regions where the integration is performed and the numerical grid for the present observer time is built. Furthermore, knowledge of the particular type of station allows the data-fitting procedure to suitably manage the retarded source points. For instance, if a partial station has to be treated, the code performs

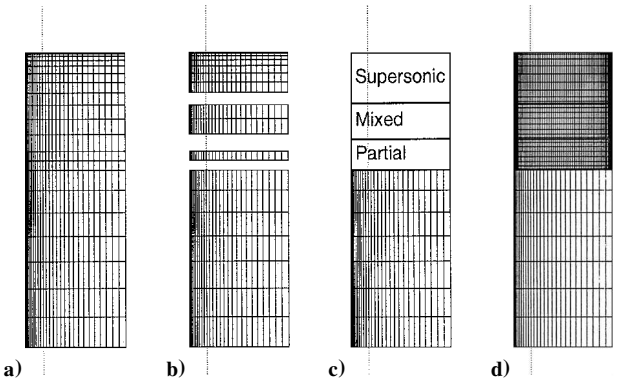

Fig. 4 By identifying the supersonic acoustic patches, the computing grid is changed from a) to d). Note the unchanged, subsonic region, where the calculations are performed on the starting mesh.

the interpolation linking the different patches into an extended section; however, a mixed station refers to a not simply connected configuration, and the interpolation has to be applied twice to build the two different patches. Note that the classification of a retarded NACA 0012 section is immediately achieved by determining the emission times of the leading edge (LE) and trailing edge (TE); in particular, both LE and TE with multiple τ^*, "supersonic"; LE with multiple τ^* and TE with a single τ^*, or vice versa, "mixed"; both LE and TE with a single τ^*, "partial":

$$\text{sign}[f_{\tau\tau}]_{\text{LE}} \neq \text{sign}[f_{\tau\tau}]_{\text{TE}}$$

and both LE and TE with a single τ^*, "single":

$$\text{sign}[f_{\tau\tau}]_{\text{LE}} = \text{sign}[f_{\tau\tau}]_{\text{TE}}$$

By using the aforementioned conditions, KURGAN performs a preliminary calculation on both blade leading and trailing edges, to identify, at the fixed observer time, the different patches constituting the retarded domain. At this stage, an essential adjustment of the interpolating procedure is the determination of the stations linking two adjacent, different patches. Figure 4 shows the starting grid (Fig. 4a) and the supersonic patches identified through the calculation of the emission times at blade LE and TE (Fig. 4b); the jumps appearing between the adjacent regions obviously depend on the adopted mesh and must be removed to avoid an inaccurate estimation of the retarded domain. Thus, the data-fitting module is invoked and iteratively used in the computation of some stations farther along the span to limit the distance between two adjacent patches to a prescribed minimum value (Fig. 4c). Once the boundaries of the supersonic patches are correctly estimated, the code may also adopt a different panelization on the various regions (Fig. 4d) and proceed to the computation of the emission times for all of the source points of the new grid.

Self-Adaptive Scheme

As already mentioned, the resulting signature arising from the integration on the acoustic surface must be devoid of any small fluctuations; otherwise, the second-time derivative outside the integral sign will provide a completely unreliable prediction of noise. An oscillating behavior may arise from an inaccurate computation of the area of the acoustic surface, or an unsuitable distribution of the retarded source points on the station. Unfortunately, this last situation often appears in the calculations and is due to a kind of flight of the source points from the critical location $(1 - M_r) = 0$. Figure 5a shows a typical acoustic surface for a hovering blade at $M_{\text{tip}} = 1.2$ and an in-plane observer location (placed at $X_{\text{obs}} = 3.23$, $Y_{\text{obs}} = 0$). In spite of the very fine grid used for the computations (300 nodes at each of the 50 spanwise stations placed outside the sonic circle), the critical region along the separation line $(1 - M_r) = 0$ appears to be not well defined. The situation may be improved by uniformly increasing the number of source points; neverthless, besides the unbearable increase of the requested CPU time, the retarded source points should be still inclined to run away from the line $(1 - M_r) = 0$,

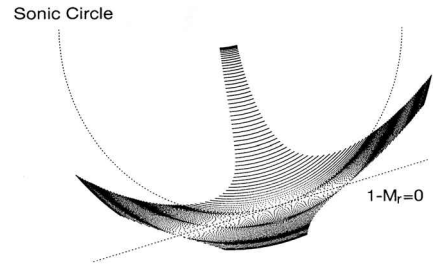

Fig. 5a Flight of the retarded source points from the critical line $(1 - M_r) = 0$.

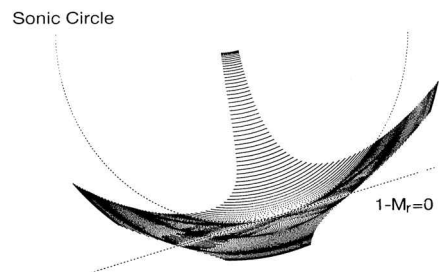

Fig. 5b Same retarded domain as Fig. 5a as improved through the self-adaptive scheme.

which represents the tangent to the sonic circle passing through the observer location.

At first glance, this behavior can probably appear to not be dangerous. However, it prevents the code from achieving any reliable numerical solution of Eqs. (2) and (4). The sparseness of the source points along the $(1 - M_r) = 0$ direction strongly depends on the observer time and the relative source–observer position; furthermore, it affects not only the geometry of the acoustic surface, but also the retarded quantities appearing in the integral kernels that, at each time step, are determined and associated with the source points. Then, a coarse distribution of the integration points may give rise to an inaccurate (and, at the worst, time oscillating) estimation of the integrals. The fluctuations that these particular conditions inevitably introduce in the computed signature are probably the main reason for the unreliable calculations usually achieved by the emission-surface algorithms. Then, at each time step, the code has to be able to change the computational domain by improving the grid resolution along the $(1 - M_r) = 0$ direction. In other words, to achieve a completely smooth signature, a self-adaptive scheme has to be used. Note that, with respect to the proposed classification of the spanwise stations, only the partial and mixed stations have to be modified because the single and the supersonic ones cannot include any critical point at $M_r = 1$.

At each partial and mixed station, KURGAN performs a preliminary computation of the retarded quantities to identify the jump nodes separating the source points with a single emission time from the ones with multiple roots. Looking at the $f(\tau)$ curve, it is clear that these nodes correspond to the source points at the minimum value of the $(1 - M_r)$ factor. Then, an iterative procedure starts to add a new source point between the i node (with a single τ) and the $(i + 1)$ node (with multiple emission times) of the numerical grid, until a prescribed minimum value of the retarded $(1 - M_r)$ factor is reached. Finally, when a critical point [satisfying the $(1 - M_r) \leq (1 - M_r)_{\text{min}}$ condition] is found, the code clusters a fixed number of nodes around it, to achieve an optimized resolution of the acoustic surface along the Doppler line $(1 - M_r) = 0$. This procedure introduces a different number of nodes at the grid stations along span; then a further interpolation has to be performed to build a regular grid and compute the integrals with a simple zero-order formulation. Figure 5b shows the improvement achieved by the self-adaptive scheme on the spatial resolution of the retarded grid along the critical Doppler line.

Swept Grids

The rectangular blade corresponds to the simplest time evolution of the acoustic surface because the presence of the straight edges ensures the existence (at each observer time) of no more than three different supersonic patches. In fact, as explained in Ref. 7, on a straight line a unique critical source point at $(1 - M_r) = 0$ may exist (per observer time), and this condition corresponds to a unique jump between a single/partial region and a mixed region. In other words, it ensures the unique presence of a particular patch on the acoustic surface. Then, moving along span from the hub to the tip and depending on the local Mach number, the supersonic patches will always appear in the sequence: single/partial → mixed → supersonic. This is very important and makes the building of the retarded domain easier: The region between two subsequent, similar stations is unequivocally identified by the type of its own spanwise boundaries.

Accounting for a swept planform, more than a critical source point may exist on the grid edges, and a complex sequence of the supersonic patches may occur. The exact distribution of the different regions strongly depends on the Mach number, the observer location, and the grid sweep. In the following, the evaluation of the quadrupole source term for a hovering rotor will be performed through the use of a two-dimensional grid provided by Brentner and reported in Ref. 9; this computing domain extends in the radial direction up to a tip Mach number of 2.286 and is characterized by a pronounced sweep. Two particular acoustic surfaces of the quadrupole grid are shown in Fig. 6. Note the presence of many different patches, whose spatial sequence changes during the revolution period and can give rise to a geometry very complex to model. The random position of the supersonic regions may produce an incorrect estimation of the different patches, especially when the starting grid has a coarse distribution of stations along span. In fact, by the computing of the emission times at the grid edges, the code can recognize the j and $j + 1$ stations as two subsequent similar stations, but the region between them can include a patch different from the boundaries' type. The incorrect identification of the supersonic regions may be avoided through a preliminary concentration of source points on the grid edges. Then, if a swept grid has to be treated, the code performs a clustering of nodes along both the grid edges and proceeds to the determination of the supersonic patches.

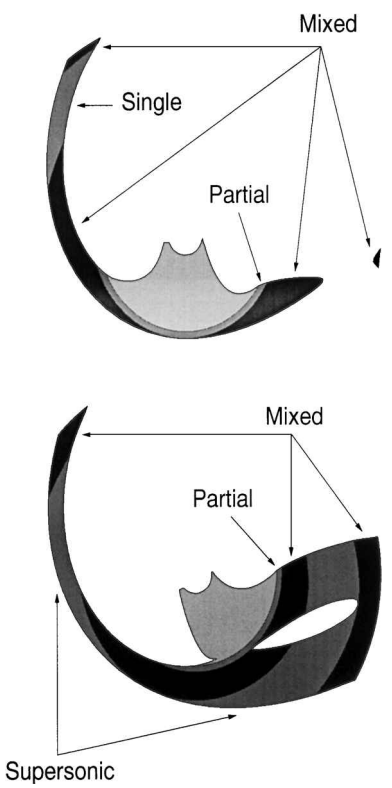

Fig. 6 Two particular retarded configurations of the quadrupole grid. Note the complexity of the acoustic domain and the accuracy achieved by the code in its own numerical reconstruction. The inner region is subsonic.

Numerical Results

This section is devoted to the numerical results achieved by KURGAN in the solution of Eqs. (2) and (4). As already mentioned, a $\frac{1}{7}$th scaled model of the hovering UH-1H rotor, with straight, untwisted blades and a NACA 0012 airfoil section, will be used. Four different tip Mach numbers ($M_{tip} = 1.05, 1.1, 1.2$, and 1.5) have been considered for the thickness noise estimation, and the numerical results are reported in Fig. 7a. The signatures have been achieved with a reduced time step (the azimuthal step is $\Delta\psi = 0.0879$ deg) and refer to an observer located in plane at 10 diameters from the center of rotation. The test cases are exactly those treated in Refs. 5 and 6; however, Wells uses a slightly different integral resolution form, where the Λ factor of Eq. (2) is assumed to be unity (thin surface approximation) and performs the integration on the blade mean surface. For completeness, Wells's results are shown in Fig. 7b. The general agreement in the resulting waveforms is very good, despite KURGAN directly solving Eq. (2) and accounting for the real, three-dimensional blade surface. Because of the presence of a singular behavior, the comparison is not as significant in terms of the predicted peak pressure value as in terms of the signature shape. From a numerical point of view, this singularity exactly corresponds to the Λ approaching zero. However, from a physical standpoint, the singularity arises because only the monopole term has been accounted for, and the calculations do not include the contribution from the loading and quadrupole source terms.

An interesting result is shown in Fig. 8, where the resulting thickness noise for the $M_{tip} = 1.5$ test case has been determined by adding the signatures arising from subsequent grid strips along span. The amplitude of the pressure disturbance decreases approaching the outer regions, whereas the peak values of the different contributions oppose each other, eventually resulting in a smooth waveform. The singularity occurs at the sonic cylinder, and moving along the span, the signature becomes wider and reduces. This behavior justifies the reduction of the acoustic pressure at the higher tip Mach numbers. Besides the good agreement with Wells' results, the fundamental feature of the supersonic thickness noise computed by KURGAN is the smoothness of the resulting waveform, which even characterizes the partial signatures shown in Fig. 8.

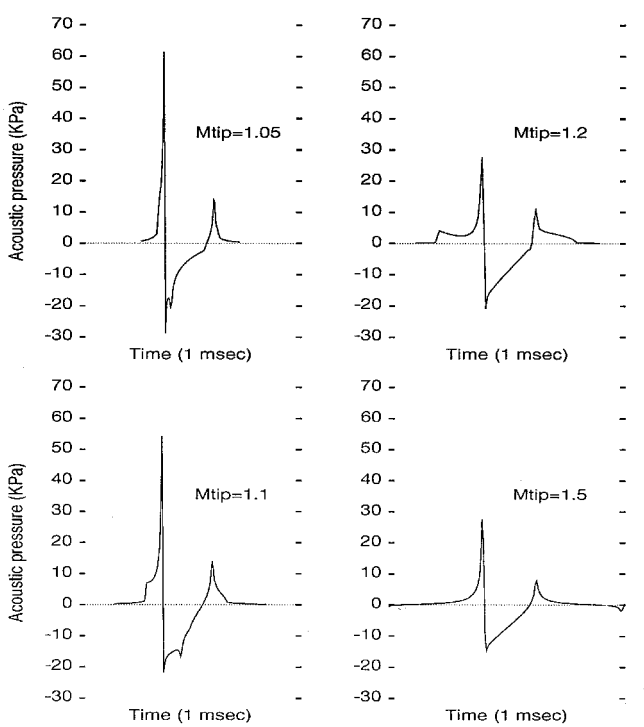

Fig. 7a Thickness noise signatures for the UH-1H hovering blade rotating at M_{tip} = 1.05, 1.1, 1.2, and 1.5, as computed by KURGAN.

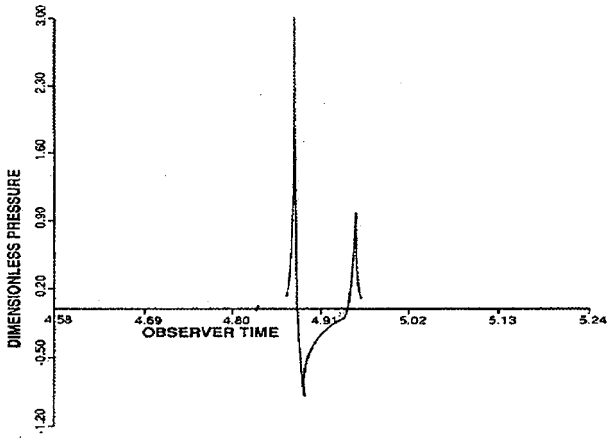

a) $M_{tip} = 1.05$

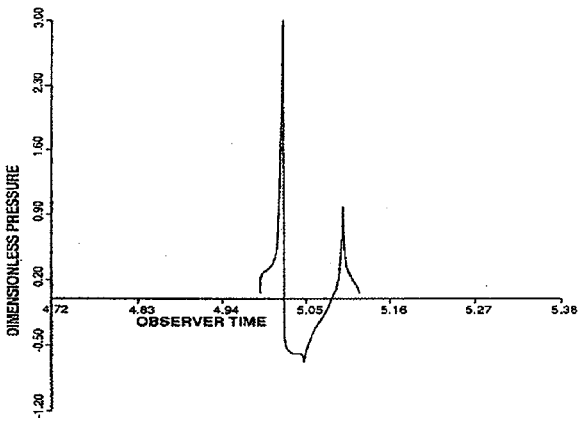

b) $M_{tip} = 1.1$

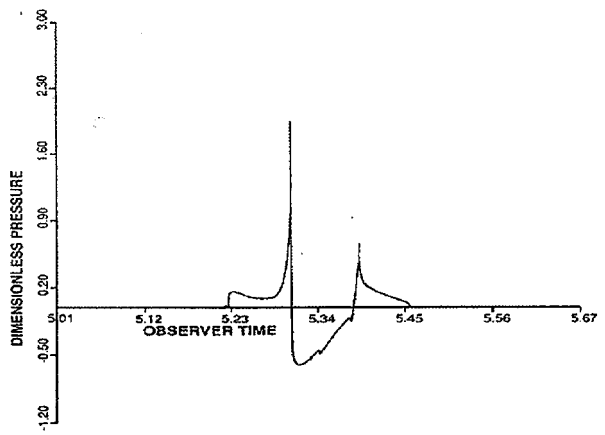

c) $M_{tip} = 1.2$

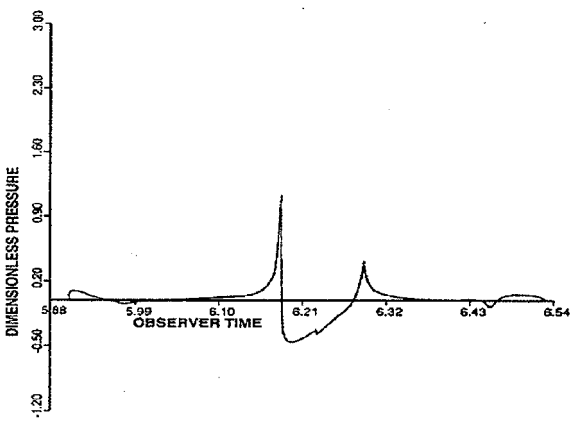

d) $M_{tip} = 1.5$

Fig. 7b Same test cases as Fig. 7a extracted from Ref. 7.

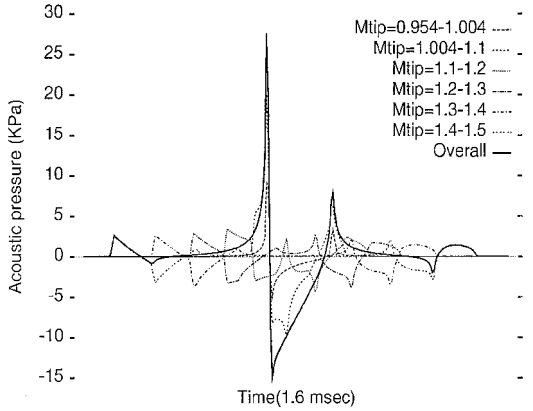

Fig. 8 Monopole term at $M_{tip} = 1.5$, as determined by adding the contributions from subsequent strips of the computing grid; different peak values contrast with each other, to provide a resulting smooth waveform.

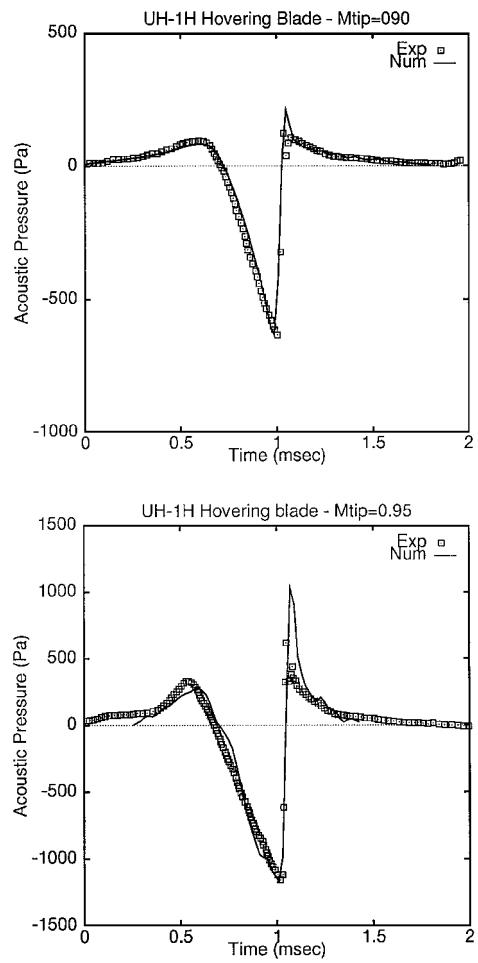

Fig. 9 Comparison between the experimental data and the KURGAN numerical predictions of noise for the UH-1H hovering blade at $M_{tip} = 0.9$ and 0.95.

The evaluation of the monopole term for the UH-1H blade rotating at a supersonic tip speed may be considered a useful academic exercise. To check the reliability of the algorithm at a more realistic operating condition, a quadrupole noise prediction has been performed through the implementation of Eq. (4), and the resulting noise waveforms have been compared with the available experimental data.[15] In particular, the surface distributions of the Q_{ij} tensor have been kindly provided by Brentner, so that the particular test cases are exactly those treated in Ref. 9. Nevertheless, this paper only includes the noise predictions for the UH-1H hovering blade at $M_{tip} = 0.9$ and 0.95: Further numerical results may be found in Ref. 16. The observer is placed in the rotor plane, at $3.09R$ from the rotor hub ($R = 1.045$ m being the rotor radius). The pronounced

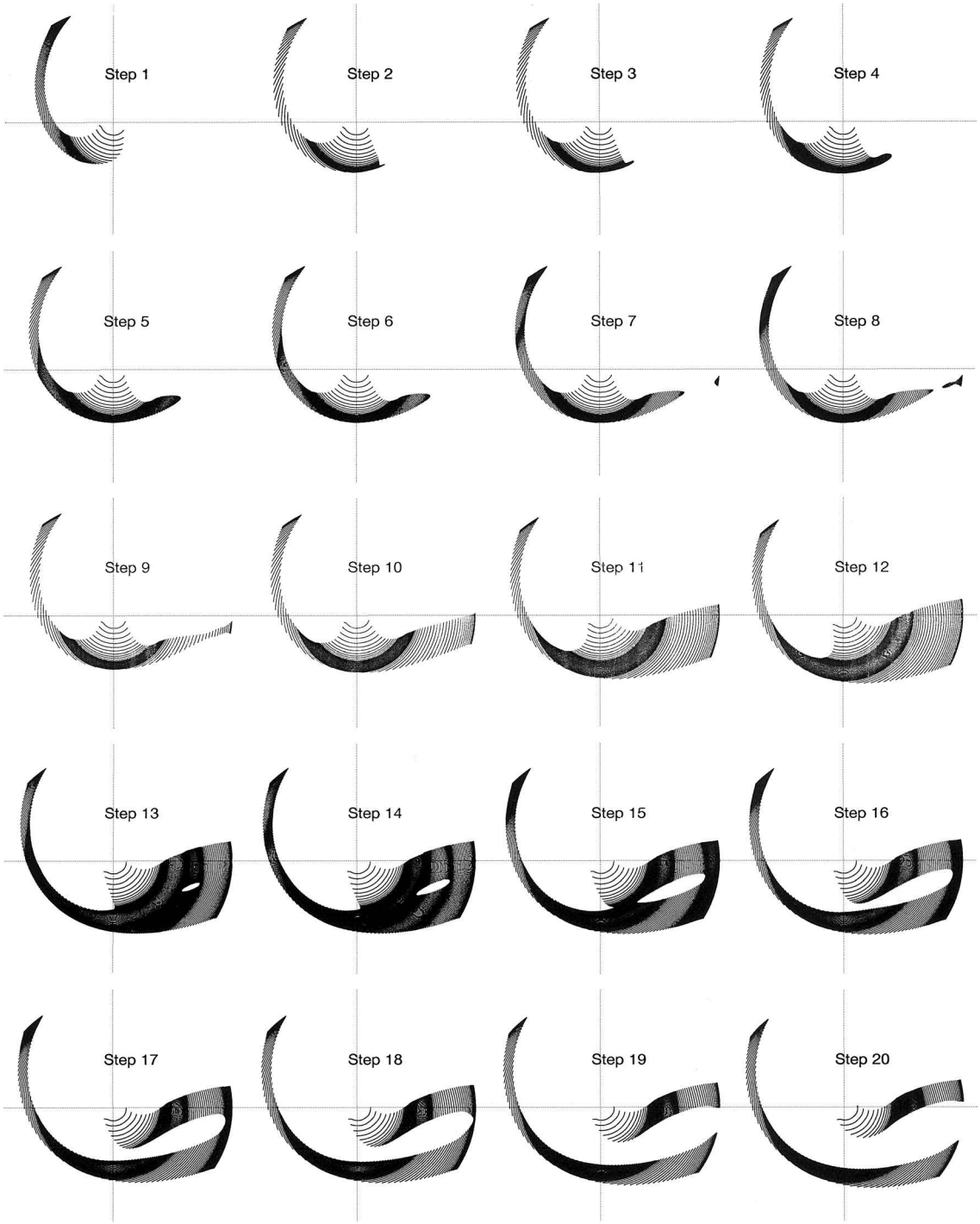

Fig. 10 Time evolution of the retarded quadrupole grid at $M_{tip} = 0.95$. Note the accuracy of the reconstruction of the acoustic domain, even at some very critical conditions (time step 2 or 7) when an unconnected patch appears, or steps 13–15, characterized by a progressively broadening hole.

sweep of the computing grid has required a concentration of 250 points along the edges to identify the supersonic patches; the calculations have been performed accounting for 1024 time steps in a revolution period ($\Delta\psi = 0.35$ deg). The comparison between the numerical and experimental results for the HSI noise prediction are shown in Fig. 9: The agreement is excellent, both for the estimated negative peak value of the acoustic pressure and the characteristic, asymmetrical shape of the resulting noise signature.

It is worthwhile to show the time evolution of the retarded quadrupole grid at $M_{tip} = 0.95$ (Fig. 10). The notable sweep of the computing grid causes an interesting development of the acoustic surface: In particular, the presence of a mixed patch outside the supersonic one causes the appearance of a kind of hole, which progressively widens (steps 13–15) to break up the most external region into two unconnected patches. From a computational point of view, further critical configurations are time steps 2 and 7, when an unconnected (spatially very limited) patch appears.

Note that the procedure also could probably be used in the Kirchhoff codes (when the integration is performed on a moving surface) because the Kirchhoff formula proposed by Farassat and Myers[17] for a supersonically moving surface requires an integration on the emission surface Σ.

Conclusions

A new algorithm to integrate the FW–H equation on a supersonic rotating domain has been presented. By using a particular classification of the retarded spanwise stations and a suitable self-adaptive scheme, the numerical procedure allows the achievement of

an accurate reconstruction of the acoustic surface outside the sonic cylinder, which accounts for the presence of the multiple emission times. The effectiveness and the reliability of the new computational tool have been tested in HSI noise predictions for a hovering blade, at some critical, delocalized conditions: The excellent agreement achieved between the experimental data and the numerical results confirm the effectiveness of the proposed algorithm in the numerical solution of the FW–H equation. In the future, the code will be extended to account for an unsteady aerodynamic input (helicopter rotor in forward flight) and will be tested on some propeller-type blade.

Acknowledgments

The author would like to express his gratitude to K. S. Brentner from NASA Langley Research Center for his kindness and courtesy in providing the quadrupole grid and the corresponding Q_{ij} tensor distributions. Furthermore, he sincerely wishes to thank E. De Bernardis. Without his guidance and continuous encouragement the numerical results included in this paper would have never been achieved.

References

[1]Ffowcs Williams, J. E., and Hawkings, D. L., "Sound Generation by Turbulence and Surfaces in Arbitrary Motion," *Philosophical Transactions of the Royal Society*, Vol. A264, No. 1151, 1969, pp. 321–342.

[2]Lyrintzis, A. S., "Review, the Use of Kirchhoff's Method in Computational Aeroacoustics," *Journal of Fluids Engineering*, Vol. 116, No. 4, 1994, pp. 665–676.

[3]Baeder, J. D., "The Role and Status of Euler Solvers in Impulsive Rotor Noise Computations," *AGARD Symposium on Aerodynamics and Aeroacoustics of Rotorcraft*, AGARD, 1994.

[4]Rahier, G., and Prieur, J., "An Efficient Kirchhoff Integration Method for Rotor Noise Prediction Starting Indifferently from Subsonically or Supersonically Meshes," *American Helicopter Society 53rd Annual Forum*, American Helicopter Society, Alexandria, VA, 1997, pp. 697–707.

[5]Wells, V. L., "Analysis of the Acoustic Planform Method for Rotor Noise Prediction," *AIAA Journal*, Vol. 26, No. 5, 1988, pp. 522, 523.

[6]Wells, V. L., "Acoustic Waveform Singularities from Supersonic Rotating Surface Sources," *AIAA Journal*, Vol. 29, No. 3, 1991, pp. 387–394.

[7]Wells, V. L., and Han, A. Y., "Geometrical and Numerical Considerations in Computing Advanced-Propeller Noise," *Journal of Aircraft*, Vol. 30, No. 3, 1993, pp. 365–371.

[8]Brentner, K. S., and Holland, P. C., "An Efficient and Robust Method for Computing Quadrupole Noise," *Journal of the American Helicopter Society*, Vol. 42, No. 2, 1997, pp. 172–181.

[9]Farassat, F., and Brentner, K. S., "Supersonic Quadrupole Noise Theory for High-Speed Helicopter Noise," *American Helicopter Society Technical Specialists' Meeting for Rotorcraft Acoustics and Aerodynamics*, American Helicopter Society, Alexandria, VA, 1997.

[10]Brentner, K. S., "Numerical Algorithms for Acoustic Integrals with Examples for Rotor Noise Prediction," *AIAA Journal*, Vol. 35, No. 4, 1997, pp. 625–630.

[11]Farassat, F., "Linear Acoustic Formulas for Calculation of Rotating Blade Noise," *AIAA Journal*, Vol. 19, No. 9, 1981, pp. 1122–1130.

[12]Farassat, F., "Theory of Noise Generation from Moving Bodies with an Application to Helicopter Rotors," NASA TR-R-451, Dec. 1975.

[13]Yu, Y. H., Caradonna, F. X., and Schmitz, F. H., "The Influence of the Transonic Flow Field on High-Speed Helicopter Impulsive Noise," 4th European Rotorcraft and Powered Lift Aircraft Forum, Paper 58, 1978.

[14]Farassat, F., and Brentner, K. S., "The Uses and Abuses of the Acoustic Analogy in Helicopter Rotor Noise Prediction," *Journal of the American Helicopter Society*, Vol. 33, No. 1, 1988, pp. 29–36.

[15]Purcell, T. W., "CFD and Transonic Helicopter Sound," Fourteenth European Rotorcraft Forum, Paper 2, Sept. 1988.

[16]Ianniello, S., "Quadrupole Noise Predictions Through the Ffowcs Williams–Hawkings Equation," *AIAA Journal*, Vol. 37, No. 9, 1999, pp. 1048–1054.

[17]Farassat, F., and Myers, M. K., "The Kirchhoff Formula for a Supersonically Moving Surface," *First Joint CEAS/AIAA Aeroacoustics Conference*, 1995.

K. Kailasanath
Associate Editor